Journal of Membrane Science 601 (2020) 117905

Contents lists available at ScienceDirect

Journal of Membrane Science

journal homepage: http://www.elsevier.com/locate/memsci

Spray-assisted layer-by-layer self-assembly of tertiary-amine-stabilized gold nanoparticles and graphene oxide for efficient CO_2 capture

Jiwoong Heo [a], Moonhyun Choi [a], Daheui Choi [a], Hyejoong Jeong [a], Hyun Young Kim [b], Hyunsik Jeon [b], Sang Wook Kang [b,**], Jinkee Hong [a,*]

[a] Department of Chemical and Biomolecular Engineering, College of Engineering, Yonsei University, 50 Yonsei-ro, Seodaemun-gu, Seoul, 03722, Republic of Korea
[b] Department of Chemistry and Energy Engineering, Sangmyung University, Seoul, 03016, Republic of Korea

ARTICLE INFO

Keywords:
Tertiary amines
Graphene oxide
Adsorptive gas separation
Layer-by-layer self-assembly (LbL)

ABSTRACT

Carbon capture and storage (CCS) is the process of capturing carbon dioxide (CO_2) produced from the combustion of fossil fuels. CO_2 is a major contributor to global warming and should be removed after combustion. The objective of this research is to design a CO_2 capture membrane consisting of tertiary-amine-stabilized gold nanoparticles (Au NPs), graphene oxide (GO), and polyelectrolytes. A high CO_2 capture ability is most important for designing a CO_2 capture membrane that can maintain a high gas permeance. Multilayer films were fabricated using an automatic spray-assisted layer-by-layer (LbL) machine. The polar affinity of polyelectrolytes assisted the CO_2 capture of tertiary amines. The randomly oriented and loosely stacked GO layers not only helped align the Au NPs in the polyelectrolyte matrix, but also helped maintain the permeance of N_2. Thus, we successfully fabricated a CO_2 adsorptive multilayer nanocoating with a maximum CO_2/N_2 selectivity of 48.48 while maintaining the N_2 permeance at 1204.25 GPU.

1. Introduction

Carbon dioxide (CO_2) is the main contributor to global warming, and most CO_2 gas is generated by the combustion of fossil fuels. The separation of CO_2 gas is an important industrial issue due to increasing concerns of global warming [1]. Recent technologies for CO_2 capture include gas absorption using polymeric liquids, solvents, and membranes, or via cryogenic processes [2–4]. Among the technologies for CO_2 removal, membrane-based CO_2 separation is remarkable owing to its high efficiency, simple operation, low energy requirements, and low cost [5–7]. To improve the performance of membrane, numerous types of mixed matrix membranes (MMMs) with nanofillers, such as metal organic frameworks (MOF), carbon materials, and inorganic fillers have been reported.

Recent studies have focused on utilizing amines as an absorbent for CO_2 [8–10]. Reversible interactions between amine groups and CO_2 gas facilitate CO_2 transport through the membrane [11,12]. Moreover, CO_2 can be captured or be transported in a facilitated manner according to the state of amine groups. CO_2 reacts with primary or secondary amines and can be transported in a facilitated manner by the reversible zwitterion reactions which are proposed by the Caplow and Danckwerts [11,12]. However, in the case of tertiary amines, CO_2 can be captured rather than be transported [13]. Tertiary amines have a higher capacity for CO_2 than hindered primary or secondary amines so that tertiary amines have been widely used for CO_2 capture application. However, the low rates of reaction impede the utilization of tertiary amines for CO_2 gas selection [13]. To overcome this, numerous research groups have attempted to improve the CO_2 capture properties by blending primary or secondary amines and tertiary amines [14,15]. However, few studies are utilizing tertiary amines for CO_2 separation membranes.

The graphene oxide (GO) membrane has been studied for its molecular sieving abilities [16,17]. GO has unique molecular barrier properties and gas selectivity [18–20]. The tortuous pathway of GO layers hinders the permeance of large molecules; therefore, by adjusting the interlayer spacing and pore size, a GO film provides a molecular sieving effect [21]. Park et al. prepared few-layered GO membranes by controlling the electrostatic repulsion and centrifugal forces during adsorption [22]. Furthermore, GO embedded in a polymer matrix functions as a gas barrier, and by controlling its embedded structure, a high selectivity can be achieved [23]. Alignment of GO in a polymeric

* Corresponding author.
** Corresponding author.
E-mail addresses: swkang@smu.ac.kr (S.W. Kang), jinkee.hong@yonsei.ac.kr, jkhong.yonsei@gmail.com (J. Hong).

https://doi.org/10.1016/j.memsci.2020.117905
Received 22 June 2019; Received in revised form 19 January 2020; Accepted 30 January 2020
Available online 4 February 2020

matrix can control the permeation of gas molecules through the membrane. A horizonal alignment with a closely packed structure inhibits the permeation of gas molecules, while a vertical alignment in a polymer matrix can facilitate gas permeation [24].

Layer-by-layer (LbL) self-assembly is an excellent candidate to fabricate functional coatings on support membranes, as it offers precise control over the thickness and interlayer structure and yields multilayered nanofilms with functional materials [25–28]. Various functional materials with molecular interactions such as electrostatic interactions, hydrogen bonding, and hydrophobic interactions can be deposited on any kind of surface. However, for application on a porous membrane support, the LbL technique should be spray-assisted, as per our previous reports. Spray-assisted LbL self-assembly not only enables the formation of multilayer films on the surface, but also provides loosely stacked and randomly aligned GO layers in the polymer matrix [29,30].

In this study, we successfully fabricated spray-assisted LbL nanofilms composed of tertiary-amine-stabilized gold nanoparticles (Au NPs), polyelectrolytes, and GO. The low reaction rate of tertiary amines, together with the polyelectrolyte matrix containing numerous polar functional groups, ensured high CO_2 capture properties. The tertiary-amine-stabilized Au NPs were evenly distributed at the interlayers of GO layers. The non-permeable properties of the GO layers aided in the alignment of Au NPs. The spray-assisted LbL technique provided randomly aligned GO layers in the polyelectrolyte matrix, so that non-polar N_2 gas could easily penetrate the loosely packed GO layers.

2. Experimental section

2.1. Materials

4-(Dimethylamino)pyridine (DMAP), gold (III) chloride trihydrate ($HAuCl_4$), tetraoctylammonium bromide (TOABr), sodium borohydride ($NaBH_4$), phosphorous pentoxide (P_2O_5), potassium persulfate ($K_2S_2O_8$), sulfuric acid (H_2SO_4), hydrogen peroxide (H_2O_2), poly(diallyldimethylammonium chloride) (MW 20–35 k, PDAC), sodium chloride (NaCl), and poly(sodium-4-styrenesulfonate) (MW 70 k, PSS) were purchased from Sigma Aldrich. Graphite (Synthetic, 74 μm, 40797) was obtained from Alfa Aesar. Sodium hydroxide (NaOH) was purchased from Daejung. A macroporous polysulfone membrane with a pore size of 0.1 μm was purchased from Toray Inc.

2.2. Preparation of GO

GO was synthesized by the modified Hummer's method [31]. Briefly, graphite powder (1.5 g), P_2O_5 (1.25 g), and $K_2S_2O_8$ (1.25 g) were dispersed in H_2SO_4 (20 mL). The solution was stirred for 5 h at 80 °C and then cooled to room temperature in an ice bath. Deionized water (DI water) (500 mL) was slowly added to the solution, following which the solution was vacuum-filtrated. When the solvent was almost filtered, it was washed with DI water (1 L). The remaining pre-oxidized graphite oxide was collected and dried at room temperature. The pre-oxidized graphite oxide powder was re-dispersed in H_2SO_4 (60 mL). The solution was cooled in an ice bath, following which $KMnO_4$ (4.5 g) was carefully and slowly added to the solution. The solution was stirred for 2 h at 35 °C, and then DI water (250 mL) was slowly added to the solution. Subsequently, it was cooled in an iced bath. The solution was then stirred for 2 h at 35 °C, following which DI water (750 mL) and H_2O_2 (7.5 mL) were added. The solution was allowed to precipitate for 24 h, and then the supernatant was removed. The precipitant was washed with 10% HCl (250 mL) and DI water (1 L) via centrifugation. Finally, gel-like GO was collected and dried at 70 °C overnight.

2.3. Preparation of DMAP-stabilized gold nanoparticles (DMAP-Au)

DMAP-stabilized Au NPs were synthesized by the phase transfer method [32]. For this, a 30 mL aqueous solution of $HAuCl_4$ (30 mM) was added to an 80 mL solution of TOABr (25 mM) in toluene. The metal salt in the aqueous phase was transferred to the toluene phase in 30 min. Subsequently, 25 mL of freshly prepared aqueous $NaBH_4$ (0.4 M) was added to the solution and vigorously stirred for 30 min. The toluene phase was collected and subsequently washed with DI water three times. Then, 80 mL of aqueous DMAP (0.1 M) was added to the solution. After 24 h, the aqueous phase of the DMAP-stabilized Au NP solution was collected.

2.4. Fabrication of spray-assisted LbL-assembled multilayer film

The DMAP-Au solution was diluted with DI water (1: 10, v: v). PDAC, PSS, and GO were dissolved in DI water at concentrations of 1 mg/mL, 1 mg/mL, and 0.5 mg/mL, respectively. The pH of GO was adjusted to 4.3 by adding NaOH (0.25 M). The salt concentrations of PDAC and PSS were adjusted to 0.1 M by adding NaCl.

The solutions were automatically sprayed using a custom-made spray machine onto the Si wafer and PSf membrane with a spray rate of 0.1 mg/mL for 30 s. The surfaces of the substrates were modified by oxygen plasma treatment (Femto Science, CUTE-1B) for 2 min to impart a negative charge and hydrophilic properties. The substrates were fixed on the spray holder in the vertical direction. The PDAC solution was sprayed for 30 s, following which DI water was sprayed for 30 s to remove unstably bound polyelectrolytes. GO, DMAP-Au, and PSS were sprayed via the same procedure. This was repeated until the desired number of tetra layers was fabricated.

2.5. Characterization

The synthesized GO was analyzed by atomic force microscopy (AFM, NX-10, Park systems). The thickness increases of the PDAC/GO/DMAP-Au/PSS multilayer films were measured by a surface profilometer (Dektak, Veeco Instruments Inc.) and cross-sectional field-emission scanning electron microscopy (FE-SEM, Carl Zeiss, SIGMA HD). The adsorption amount of each component was analyzed using a quartz crystal microbalance (QCM, Stanford Research Systems, Sunnyvale). The fabricated membranes were analyzed by X-ray photoelectron spectroscopy (XPS, K-alpha+, ThermoFisher Scientific). The internal structure of the multilayer film was analyzed by cross-sectional high-resolution transmission electron microscopy (HR-TEM, JEM-F200, JEOL). The zeta-potential values of GO solution were measured by dynamic light scattering (DLS, SZ-100, Horiba).

2.6. Gas selectivity measurements

The gas permeance was measured using a circular stainless-steel separation module. The effective membrane area was 4.9 cm^2. The permeance of single gases (N_2 and CO_2) was measured with a specific pressure (1 bar) at room temperature using a Gilibrator bubble flow meter (Gilian Instruments, Clearwater, IL, USA). The permeance was presented in units of GPU [$1\ \text{GPU} = 1 \times 10^{-6}\ \text{cm}^3\ (\text{STP})/(\text{cm}^2\ \text{s cm Hg})$]. The membranes were mounted inside the permeation test cell with the selective layer facing the feed gas. The permeation flux (J) was calculated from the volume of permeate gas (V) over a given time (s), permeation area (cm^2), and given pressure (cm Hg):

$$J = \frac{V}{AtP} \quad (1)$$

where V is volume of permeate gas, A is the membrane area for permeation, t is time, and P is given pressure.

3. Results and discussion

Fig. 1 schematically illustrates the composite membrane. The selective layers were LbL-assembled by repeating tetra layers composed of

PDAC, GO, DMAP-Au, and PSS. The driving force for LbL self-assembly was electrostatic interactions [33]. The LbL film notation used here is $(PDAC/GO/DMAP\text{-}Au/PSS)_n$, where n represents the number of tetra layers. PDAC, GO, DMAP-Au, and PSS were sequentially adsorbed until the desired amount of tetra layers was deposited. The surface of the Au NPs partially positively charged by the DMAP. The Au $4f_{7/2}$ regions of the XPS spectra for the $(PDAC/PSS)_{25}(PDAC/GO/DMAP\text{-}Au/PSS)_{10}$ film is indicative of the chemical environment surrounding the gold and can provide information of the surface charge of the gold nanoparticle (Fig. S1). The binding energy of the $4f_{7/2}$ orbital of the DMAP-Au NPs was 83.98 eV, while the reported average value of gold NPs was 83.5 eV. The value was slightly increased because the surface of the gold nanoparticles was partially positively charged by the DMAP. It has been reported that partially positively charged surface of metal nanoparticles interacts with CO_2 molecules. The zeta-potential value of DMAP-Au NPs was 37.4 mV. Consequently, DMAP stabilized Au NPs enabled not only a stable aqueous dispersion of Au NPs but also attractive interaction with CO_2 molecules.

The role of GO is to align DMAP-Au in the polyelectrolyte matrix. The thickness of the synthesized GO was approximately 1 nm, and the lateral size of the GO sheet was random, from tens of nanometers to several microns (Fig. S2). DMAP-Au was adsorbed onto the GO sheets via electrostatic interactions between the positively charged amine groups of DMAP-Au and carboxyl groups of GO. As the LbL film deposition of NPs and polyelectrolytes involves the rearrangement of NPs in the polyelectrolyte matrix, NPs could have aggregated in the polyelectrolyte matrix. The GO layers prevent the severe aggregation of NPs by aligning DMAP-Au NPs onto the sheet surfaces. The polyelectrolyte layers are composed of PDAC and PSS, which have numerous polar functional groups such as quaternary ammonium (N^+) and sulfonate (SO_3^-) groups. The polar affinity of the polyelectrolyte layer assists the tertiary amine group in capturing CO_2 gas molecules. The base layers consist of 25 bilayers of PDAC and PSS, which facilitate the stable deposition of selective layers.

It is essential to choose a coating method for gas separation. From the viewpoint of industrial application, the spray-assisted LbL method is more suitable than the conventional dipping method owing to its automated procedure and high efficiency. Furthermore, conventional LbL assembly cannot form a stable film on a porous membrane surface. During dipping, the polyelectrolytes penetrate the membrane, making washing difficult and causing severe aggregation of GO on the membrane surface. Therefore, we chose the automatic spray-assisted LbL method and successfully fabricated multilayer nanofilms on the porous membrane support. The spray-assisted LbL method also provides a randomly oriented GO structure in the polyelectrolyte matrix. The sprayed solutions form small droplets containing polyelectrolytes, GO, or DMAP-Au NPs on the surface of the membrane. Subsequently, the small droplets coalesce into a larger droplet until a fully covered surface is formed. The unique adsorption mechanism of spray-assisted LbL self-assembly leads to the formation of randomly oriented GO layers in the polyelectrolyte layer. The interlayer structure of the multilayer film is discussed later.

The thickness of the multilayer thin film was precisely controlled by adjusting the number of tetra layers (Fig. 2A). The pH of the GO suspension and salt concentration of the polyelectrolytes are important to determine the thickness of the multilayer film. At pH 4.3, the GO

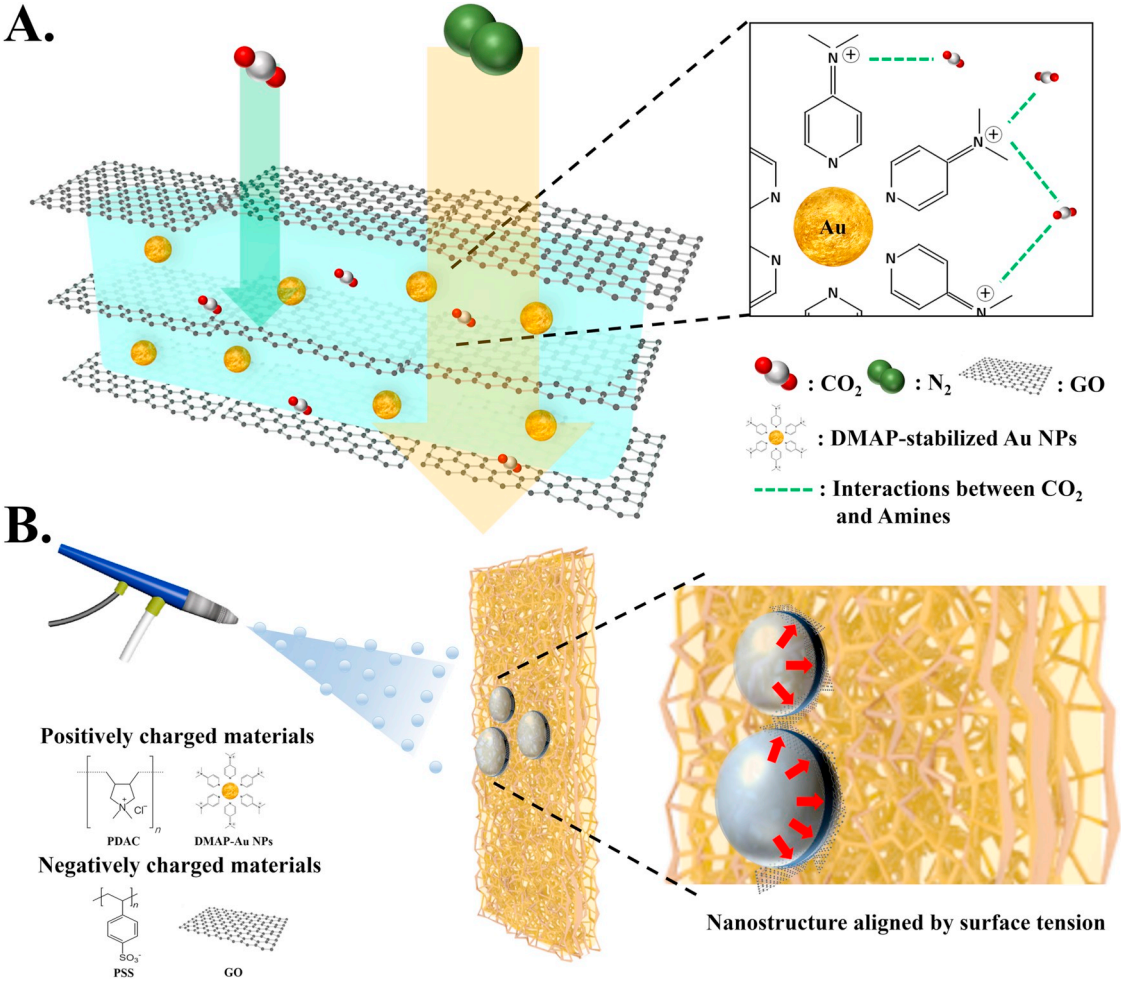

Fig. 1. Schematic illustration of the structure of the multilayer film (A) and spray-assisted layer-by-layer self-assembly method.

carboxyl groups of GO are properly deprotonated, which offers sufficient charge density for LbL assembly [34]. The zeta potential value of GO at pH 4.3 was −45.7 mV. The salt concentration of the polyelectrolyte solution was determined based on our previous research [35,36]. Excess salt concentration causes unfavorable gas leakage, while a too low salt concentration results in insufficient polyelectrolyte adsorption. The thickness of the base layer of $(PDAC/PSS)_{25}$ was chosen as 60 nm. If the thickness of the base layer is lower than 60 nm, gas permeance occurs too rapidly to measure with the bubble flowmeter; on the other hand, if the base layer is too thick, it reduces the overall gas permeance. QCM analysis indicated the successful deposition of multilayer films, and provided the mass ratio of each component in the multilayer films (Fig. 2B). The calculated mass ratio of PDAC: GO: Au: PSS was 16: 11: 4: 3. The multilayer film mainly comprises polyelectrolytes; these results agree with the schematic illustration in Fig. 1A, where the GO and DMAP-Au NPs are distributed in the polyelectrolyte matrix. The cross-sectional SEM images (Fig. 2C and D) revealed a distinct boundary between the base layer and selective layer. Moreover, the multilayer film was deposited onto the substrate, not inside the pores of the PSf support membrane.

The surface morphologies of the films were analyzed by SEM (Fig. 3). A uniform distribution of DMAP-Au NPs was observed on the surface without any cracks. As the kinetic diameters of CO_2 and N_2 are 0.33 nm and 0.364 nm, respectively, if there is a pore, the membrane loses its selectivity due to gas leakage. Moreover, the evenly distributed DMAP-Au NPs on the surface offer a large surface area for the reaction between the tertiary amine groups of DMAP and CO_2. The wrinkled, rough surface was formed due to the unique adsorption kinetics of spray-assisted LbL self-assembly. Randomly oriented GO sheets, Au NPs, and polyelectrolytes formed a rough surface, resulting in an increased surface area to thereby allow gas molecules to permeate easily.

The cross-sectional HRTEM image revealed the interlayer structure of the multilayer film (Fig. 4A and B). The DMAP-Au NPs did not aggregate in the polyelectrolyte matrix, but evenly aligned on the surface of the GO sheets. The GO sheets were randomly oriented with a loosely packed structure. The randomly and loosely stacked GO layers enable high N_2 permeance. Furthermore, the cross-sectional HRTEM images revealed that the DMAP-Au NPs were evenly distributed not only in the horizontal direction but also in the vertical direction, ensuring a high surface area for CO_2 to react with the tertiary amines of DMAP-Au NPs. The green circles in Fig. 4B represent evenly distributed DMAP-Au NPs in the polyelectrolyte matrix, and the red lines show the direction of the randomly oriented GO sheets. The DMAP-Au NPs were aligned by the GO sheets such that internal rearrangement was inhibited, resulting in an even distribution of Au NPs in the vertical direction.

The gas separation performance was measured using the bubble flow meter (Table 1). Each permeance data was measured four times, and the average value was listed in Table 1. Twenty-five bilayers of the base layer $(PDAC/PSS)_{25}$ exhibited a selectivity (CO_2/N_2) of 3.64 due to the polar affinity of PDAC and PSS and facilitated CO_2 transport via the amine-mediated reversible reaction [36]. Even though the base layer of $(PDAC/PSS)_{25}$ represented facilitated CO_2 transport, the main selectivity would result from the selective layer, which has CO_2 capture ability. CO_2 molecules were already strongly captured at the selective layer so that amine groups of base layers didn't have the chance to facilitate CO_2 transport. When the selective layers were coated onto the base layer, CO_2 was captured by the tertiary amine groups of the DMAP-Au NPs, introducing N_2/CO_2 selectivity. The permeances of each gas were measured in a single gas condition.

Tertiary amines have a high capacity of CO_2 compared with other kinds of amines such as primary amines and secondary amines. However, tertiary amines have a low reaction rate, which limits their application in gas separation. The polyelectrolyte matrix, which has a high density of polar functional groups, aids the reaction between CO_2

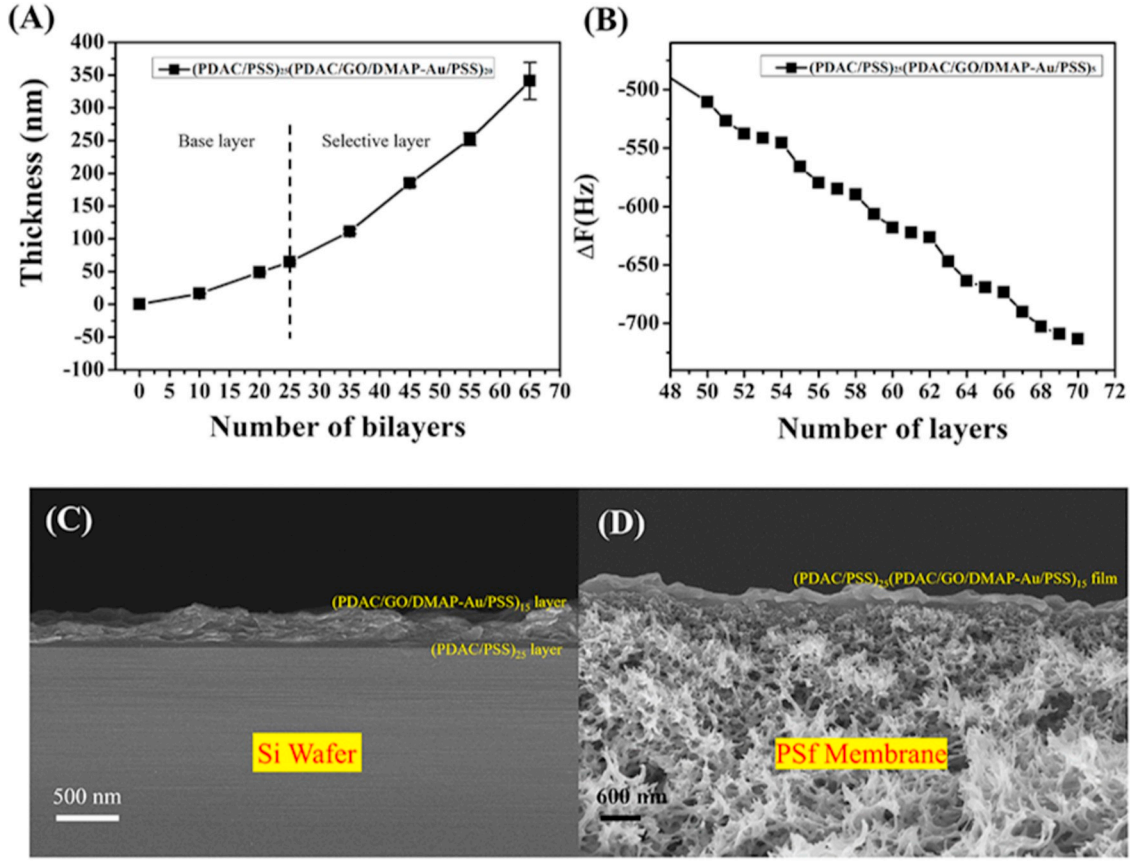

Fig. 2. (A) Thickness growth curve, (B) QCM analysis and cross-sectional SEM images of the multilayer film on (C) Si wafer and (D) PSf membrane.

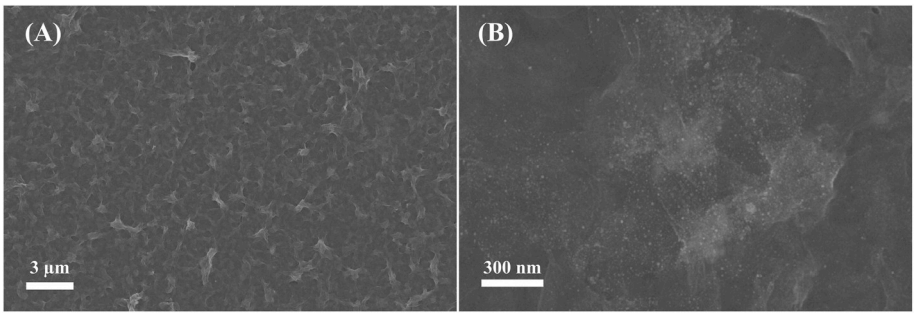

Fig. 3. Top-view SEM images of the multilayer film in (A) low magnification and (B) high magnification.

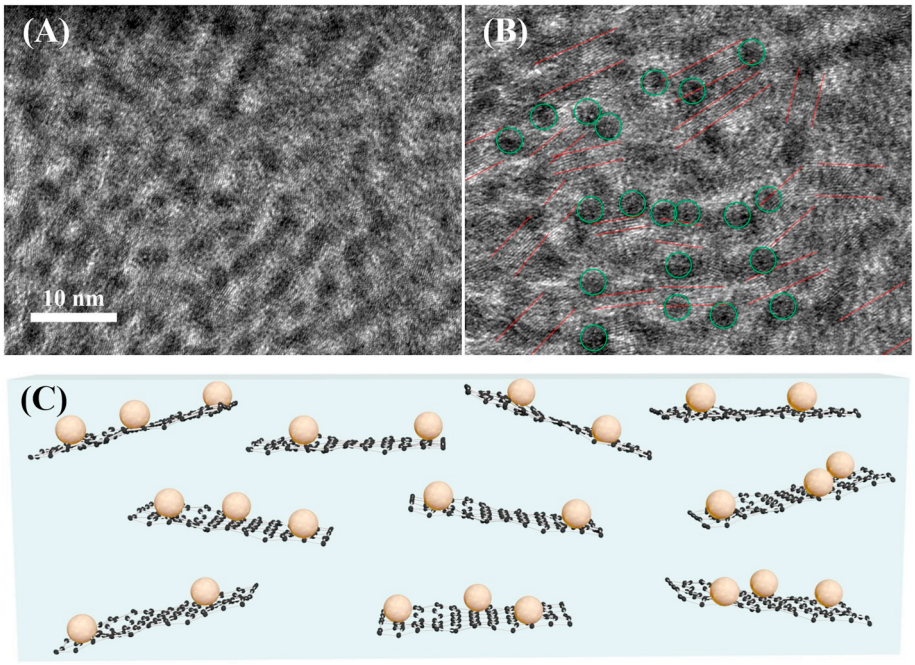

Fig. 4. (A) Cross-sectional TEM image of the selective layer and (B) with schematic illustrations of the DMAP-Au NPs and GO layers. The green circles represent aligned DMAP-Au NPs and red lines represent the randomly and loosely stacked GO layers. (C) Schematic illustration of the structure of the multilayer film. (For interpretation of the references to colour in this figure legend, the reader is referred to the Web version of this article.)

Table 1
CO_2 and N_2 gas permeance and selectivity of the multilayer films.

Membranes	Permeance (GPU)		Selectivity	
	CO_2	N_2	CO_2/N_2	N_2/CO_2
$(PDAC/PSS)_{25}$	54.03	14.86	3.64	0.28
$(PDAC/PSS)_{25}$ $(PDAC/GO/DMAP\text{-}Au/PSS)_5$	42.58	403.84	0.11	9.48
$(PDAC/PSS)_{25}$ $(PDAC/GO/DMAP\text{-}Au/PSS)_{10}$	24.84	1204.26	0.02	48.48

and tertiary amines. Although the GO sheets were loosely and randomly stacked, the CO_2 gas molecules, which are attracted by the DMAP-Au NPs, should travel through the torturous pathway of the aligned GO sheets, compared to non-polar N_2 molecules which can permeate without any hindrance.

As the thickness of the selective layer increased, the permeance of N_2 also increased. Generally, the mass transfer would be decreased as the thickness of the film is increased. However, in the case of the spray-assisted LbL self-assembly systems, as the LbL cycles were repeated, we hypothesized that the film became more permeable due to the rearrangement phenomenon of the film during the process. This hypothesis can be further confirmed by the cross-sectional TEM image. We can see loosely and randomly packed GO and DMAP-Au structure. Loosely and randomly incorporated GO sheets in the polymer matrix can enhance the permeance of the gas molecules while the densely packed GO layers block the transport of the gas molecules. As a result, the electrically neutral N_2 gas molecules can easily penetrate multilayer film along the frictionless smooth surface of GO sheets. However, in the case of CO_2, as the thickness of the film is increased, the quantities of tertiary amine also increased, resulting in more effective CO_2 capture.

The maximum N_2/CO_2 selectivity of 48.48 was achieved when the thickness of the selective layer was 200 nm. It is difficult to achieve both high selectivity and high permeance; however, in this study, the permeance of N_2 gas was maintained over 1000 GPU by using a thin film, loosely stacked GO sheets, and owing to the non-polar characteristics of N_2 gas. The long-term stability of the selective membrane also tested (Fig. S3). The membrane that is used in the long-term stability test was $(PDAC/PSS)_{25}(PDAC/GO/DMAP\text{-}Au/PSS)_5$. Initial N_2/CO_2 selectivity was 9.48 and it decreased to 5 after 7 days. The N_2/CO_2 selectivity maintained around 5. The initial N_2 permeance was 403.84 GPU and it increased to 760 GPU due to slightly decreased stability of the membrane. Even though the results represented slightly decreased selectivity, the selectivity maintained above 5 for a week. Furthermore,

membrane performance with the high-pressure condition was investigated (Fig. S4). N_2/CO_2 selectivity of $(PDAC/PSS)_{25}(PDAC/GO/DMAP\text{-}Au/PSS)_5$ membrane at 3 bars was 9.59 with CO_2 and N_2 permeance of 3.08 GPU and 29.54 GPU, respectively. The selectivity was similar to the selectivity at 1 bar condition, however, the gas permeance was decreased. The membrane has loosely and randomly incorporated GO sheets in the polymer matrix so that structure might be compressed by the high pressure resulting in reduced gas permeance.

4. Conclusion

In conclusion, we successfully fabricated a multilayer film with high N_2/CO_2 selectivity via the spray-assisted LbL self-assembly method. The automated spray-assisted LbL self-assembly method is suitable for industrial applications. Electrostatic interactions served as the driving force for LbL assembly. The QCM provided the mass ratio of the components of the multilayer film. The polar affinity of the polyelectrolytes aided in the CO_2 capture of DMAP-Au NPs. The randomly oriented and loosely packed GO layers not only helped align the DMAP-Au NPs in the polyelectrolyte matrix, but also helped maintain the permeance of N_2. Finally, the maximum N_2/CO_2 selectivity of 48.48 was achieved by depositing ten tetra layers of the selective layers.

Declaration of competing interest

The authors declare that they have no known competing financial interests or personal relationships that could have appeared to influence the work reported in this paper.

CRediT authorship contribution statement

Jiwoong Heo: Writing - original draft, Writing - review & editing, Formal analysis. **Moonhyun Choi:** Formal analysis, Data curation. **Daheui Choi:** Formal analysis, Writing - review & editing. **Hyejoong Jeong:** Data curation, Writing - review & editing. **Hyun Young Kim:** Formal analysis, Writing - review & editing. **Hyunsik Jeon:** Writing - review & editing, Data curation. **Sang Wook Kang:** Writing - original draft, Writing - review & editing. **Jinkee Hong:** Supervision, Conceptualization, Writing - original draft, Writing - review & editing.

Acknowledgment

This research was supported by Basic Science Research Program through the National Research Foundation of Korea (NRF) funded by the Ministry of Science and ICT (NRF-2017R1E1A1A01074343).

Appendix A. Supplementary data

Supplementary data to this article can be found online at https://doi.org/10.1016/j.memsci.2020.117905.

References

[1] E.M. Maya, D.M. Muñoz, G. José, J. de Abajo, Á.E. Lozano, Thermal effect on polyethyleneoxide-containing copolyimide membranes for CO2/N2 separation, Desalination 199 (2006) 188–190.
[2] A.L. Ahmad, A.R. Sunarti, K.T. Lee, W.J.N. Fernando, CO2 removal using membrane gas absorption, Int. J. Greenh. Gas Contr. 4 (2010) 495–498.
[3] M. Hasib-ur-Rahman, M. Siaj, F. Larachi, Ionic liquids for CO2 capture—development and progress, Chem. Eng. Process 49 (2010) 313–322.
[4] B. Belaissaoui, Y. Le Moullec, D. Willson, E. Favre, Hybrid membrane cryogenic process for post-combustion CO2 capture, J. Membr. Sci. 415 (2012) 424–434.
[5] A.L. Khan, X. Li, I.F. Vankelecom, Mixed-gas CO2/CH4 and CO2/N2 separation with sulfonated PEEK membranes, J. Membr. Sci. 372 (2011) 87–96.
[6] R. Carapellucci, A. Milazzo, Membrane systems for CO2 capture and their integration with gas turbine plants, Proc. Inst. Mech. Eng. 217 (2003) 505–517.
[7] M. Choi, J. Heo, H. Kim, S.W. Kang, J. Hong, Control of gas permeability by transforming the molecular structure of silk fibroin in multilayered nanocoatings for CO2 adsorptive separation, J. Membr. Sci. 573 (2019) 554–559.
[8] I. Erucar, S. Keskin, High CO2 selectivity of an amine-functionalized metal organic framework in adsorption-based and membrane-based gas separations, Ind. Eng. Chem. Res. 52 (2013) 3462–3472.
[9] R.W. Flaig, T.M. Osborn Popp, A.M. Fracaroli, E.A. Kapustin, M.J. Kalmutzki, R. M. Altamimi, F. Fathieh, J.A. Reimer, O.M. Yaghi, The chemistry of CO2 capture in an amine-functionalized metal–organic framework under dry and humid conditions, J. Am. Chem. Soc. 139 (2017) 12125–12128.
[10] F. Su, C. Lu, S.C. Kuo, W. Zeng, Adsorption of CO2 on amine-functionalized Y-type zeolites, Energy Fuels 24 (2010) 1441–1448.
[11] M. Caplow, Kinetics of carbamate formation and breakdown, J. Am. Chem. Soc. 90 (1968) 6795–6803.
[12] P.V. Danckwerts, The reaction of CO2 with ethanolamines, Chem. Eng. Sci. 34 (1979) 443–446.
[13] F.A. Chowdhury, H. Yamada, T. Higashii, K. Goto, M. Onoda, CO2 capture by tertiary amine absorbents: a performance comparison study, Ind. Eng. Chem. Res. 52 (2013) 8323–8331.
[14] R.J. Littel, G.F. Versteeg, W.P.M. Van Swaaij, Kinetics of CO2 with primary and secondary amines in aqueous solutions—I. Zwitterion deprotonation kinetics for DEA and DIPA in aqueous blends of alkanolamines, Chem. Eng. Sci. 47 (1992) 2027–2035.
[15] G. Kumar, T.K. Mondal, M. Kundu, Solubility of CO2 in aqueous blends of (Diethanolamine+ 2-Amino-2-methyl-1-propanol) and (Diethanolamine+ N-methyldiethanolamine), J. Chem. Eng. Data 57 (2012) 670–680.
[16] R.K. Joshi, P. Carbone, F.C. Wang, V.G. Kravets, Y. Su, I.V. Grigorieva, H.A. Wu, A. K. Geim, R.R. Nair, Precise and ultrafast molecular sieving through graphene oxide membranes, Science 343 (2014) 752–754.
[17] J. Shen, G. Liu, K. Huang, Z. Chu, W. Jin, N. Xu, Subnanometer two-dimensional graphene oxide channels for ultrafast gas sieving, ACS Nano 10 (2016) 3398–3409.
[18] Y.H. Yang, L. Bolling, M.A. Priolo, J.C. Grunlan, Super gas barrier and selectivity of graphene oxide-polymer multilayer thin films, Adv. Mater. 25 (2013) 503–508.
[19] J. Tanum, H. Jeong, J. Heo, M. Choi, K. Park, J. Hong, Assembly of graphene oxide multilayer film for stable and sustained release of nitric oxide gas, Appl. Surf. Sci. 486 (2019) 452–459.
[20] S. Jung, U. Han, J. Hong, Chemical and physical modification of layer-by-layer assembled nanofilms composed of block copolymer micelles and graphene oxide for controlled drug release, J. Ind. Eng. Chem. 56 (2017) 413–421.
[21] Y. You, V. Sahajwalla, M. Yoshimura, R.K. Joshi, Graphene and graphene oxide for desalination, Nanoscale 8 (2016) 117–119.
[22] H.W. Kim, H.W. Yoon, S.M. Yoon, B.M. Yoo, B.K. Ahn, Y.H. Cho, H.J. Shin, H. Yang, U. Paik, S. Kwon, J.Y. Choi, H.B. Park, Selective gas transport through few-layered graphene and graphene oxide membranes, Science 342 (2013) 91–95.
[23] X. Li, L. Ma, H. Zhang, S. Wang, Z. Jiang, R. Guo, H. Wu, X.Z. Cao, J. Yang, B. Wang, Synergistic effect of combining carbon nanotubes and graphene oxide in mixed matrix membranes for efficient CO2 separation, J. Membr. Sci. 479 (2015) 1–10.
[24] J. Abraham, K.S. Vasu, C.D. Williams, K. Gopinadhan, Y. Su, C.T. Cherian, J. Dix, E. Prestat, S.J. Haigh, I.V. Grigorieva, P. Carbone, A.K. Geim, R.R. Nair, Tunable sieving of ions using graphene oxide membranes, Nat. Nanotechnol. 12 (2017) 546.
[25] G. Decher, Fuzzy nanoassemblies: toward layered polymeric multicomposites, Science 277 (1997) 1232–1237.
[26] H. Jeong, K. Park, J.C. Yoo, J. Hong, Structural heterogeneity in polymeric nitric oxide donor nanoblended coatings for controlled release behaviors, RSC Adv. 8 (2018) 38792–38800.
[27] S. Park, H. Kim, S. Yang, J. Moon, H. Ahn, J. Hong, A Polysaccharide-based antibacterial coating with improved durability for clear overlay appliances, ACS Appl. Mater. Interfaces 10 (2018) 17714–17721.
[28] D. Choi, M. Komeda, J. Heo, J. Hong, M. Matsusaki, M. Akashi, Vascular endothelial growth factor-incorporated multilayer film induces pre-angiogenesis in endothelial cells, ACS Biomater. Sci. Eng. 4 (2018) 1833–1842.
[29] J. Heo, H. Jeong, J. Hong, CO2 bubble assisted layer-by-layer self-assembly of graphene oxide multilayer film, Colloids Surf., A 533 (2017) 76–80.
[30] S.Y. Kim, J. Hong, R. Kavian, S.W. Lee, M.N. Hyder, Y. Shao-Horn, P.T. Hammond, Rapid fabrication of thick spray-layer-by-layer carbon nanotube electrodes for high power and energy devices, Energy Environ. Sci. 6 (2013) 888–897.
[31] W. Li, F. Li, H. Li, M. Su, M. Gao, Y. Li, D. Su, X. Zhang, Y. Song, Flexible circuits and soft actuators by printing assembly of graphene, ACS Appl. Mater. Interfaces 8 (2016) 12369–12376.
[32] D.I. Gittins, F. Caruso, Spontaneous phase transfer of nanoparticulate metals from organic to aqueous media, Angew. Chem. Int. Ed. 40 (2001) 3001–3004.
[33] R. Zhang, Y. Zhang, H.S. Antila, J.L. Lutkenhaus, M. Sammalkorpi, Role of salt and water in the plasticization of PDAC/PSS polyelectrolyte assemblies, J. Phys. Chem. B 121 (2016) 322–333.
[34] B. Konkena, S. Vasudevan, Understanding aqueous dispersibility of graphene oxide and reduced graphene oxide through pKa measurements, J. Phys. Chem. Lett. 3 (2012) 867–872.
[35] J. Heo, J. Hong, Effects of CO2 bubbles on layer-by-layer assembled hybrid thin film, Chem. Eng. J. 303 (2016) 433–438.
[36] J. Heo, M. Choi, J. Chang, D. Ji, S.W. Kang, J. Hong, Highly permeable graphene oxide/polyelectrolytes hybrid thin films for enhanced CO 2/N 2 separation performance, Sci. Rep. 7 (2017) 456.